Journal of the Korean Society of Marine Engineers, Vol.28, No.8, pp.1258~1269, 2004. 11 (ISSN 1226-9549)

Numerical Calculation of Flow Pattern and Fluid Force on a Circular Arc-type Sea Anchor

Ki-Deok Ro† · Se-Kyung Oh*

(Manuscript : Received OCT. 11, 2004 ; Revised NOV. 10, 2004)

Abstract : The fluid dynamic characteristics of a circular arc type sea anchor were calculated by a discrete vortex method. The flow for the surface of the sea anchor was represented by arranging bound vortices at adequate intervals. The simulations were performed by assuming that the separations occur at edges. With time, the drag coefficient was almost constant but the lift coefficient oscillated in a cycle due to von Karman's vortex street. As the camber ratios increase, the drag coefficient and Strouhal number were almost constant but the oscillating amplitude of the lift coefficient increased largely.

Key words : Fluid Dynamics, Numerical Analysis, Unsteady Flow, Separation, Vortex Method, Sea Anchor

Nomenclatures

B : camber or integral path
C : chord of the sea anchor
C_D : drag coefficient
C_L : lift coefficient
F(z) : complex potential
i : imaginary number ($=\sqrt{-1}$)
j : bound vortex
ℓ : free vortex
m : numbers of bound vortices
n : numbers of free vortices
R : radius of curvature
r : radius of the vortex
St : Strouhal number
t : time
Δt : time step
U : uniform flow
W : complex velocity
X : component of force for x direction
Y : component of force for y direction
z : complex number ($=x+iy$)
θ : angle of inclination
κ : strength of vortex
ρ : density of fluid
σ : radius of viscous core

† Corresponding Author (School of Mechanical and Aerospace Engineering · Institute of Marine Industry, Gyeongsang National University), E-mail : rokid@gaechuk.gsnu.ac.kr, Tel : 055)640-3123
* School of Mechanical and Aerospace Engineering · Institute of Marine Industry, Gyeongsang National University

v_θ : induced velocity
Ψ : stream function
Ψ_0 : stream function at the surface
$\overline{\ }$: complex conjugate
~ : free vortex
· : time difference

1. Introduction

Squid angling(Lee, Park and Kim, 1985) is done by attracting highly phototactic squid using fishing lamps strung around a fishing boat and raising and loweing long fishing lines equipped with many artificial bait pieces using manual or automatic squid angling machine to lure the voracious squid. When caught by the moving fishing lines, the squid are struck onto the fishing boat. The velocity of the fishing boat floating on the water should be the same as that of fishing lines, so that the shade of the fishing boat covers the fishing lines for easier luring squids and the fishing lines do not become tangled, enabling on-going work. The velocity of the floating fishing lines is the same as that of the marine flow, while the fishing boat doesn't have the same velocity due to air resistance. To make the fishing boat and fishing lines move at the same velocity, sea anchors(Cho, 1989) in a parachute shape should be spread in the water at a right angle to the water flow, so that hydrodynamic resistance allows the fishing boat to move at the same velocity as the marine flow. There are approximately 6,000 squid-angling boats in Korean waters. However, the sea anchors used for the boats are not designed with consideration for fluid dynamics and are often made by manufacturers without scientific design concepts. As a result, they are considerably larger than their fishing boats. As well, their shape is not kept constant due to their improper spread. In some cases, they are torn by the dynamic imbalance resulting from the strong eddy flow around them. Studies on sea anchors have not been conducted in Korea, and the only study on the resistance of a sea anchor in the water is found in Japan (Nomura, Mori, Tawara and Osawa, 1967)

This study was purposed to suggest elementary data for a design of highly efficient sea anchors by investigating the flow pattern, drag, and lift around the sea anchors using a discrete vortex method. This method is used to analyze a flow field by tracing the movement of each vortex filament, on the assumption that an area with a high concentration of vorticity is an assemblage of many vortex filaments. It has been widely used to analyze various types of flow fields because this method offers easier modeling of the flow and understanding of the physical meanings than do either the finite difference method or finite element method. In addition, this method does not need the formation of a lattice and enables a simulation by a simple calculation.

In the discrete vortex method, the flow around an object is analyzed by mapping it to the flow around a circular cylinder(Kuwahara, 1973: Sarpkaya, 1986: and Sung, Kim and Hyun, 1994). However, since this process requires the deduction of a function for each object, it is very

complicated, and thus impractical. When analyzing a complex surface on an object, therefore, the surface is approximated at a fixed number of bound vertices and the results are combined with the discrete vortex method (Inamuro, Saito and Adachi, 1984: Ro, 1993: Ro, 2000: Tsutahara, Kimura and Ro, 1989: and Tsutahara, Kimura and Ro, 1994).

The latter method was used in this study for the convenience of calculation. Although the discrete vortex method had originally been developed to analyze the flow field of an unsteady separate flow of which the Reynolds number is high, the viscous diffusion effects of fluid has been represented by the core-spreading method (Inamuro, Saito and Adachi, 1984), random-walk method (Chorin, 1982: and: Ro and Tsutahara. 1997), and diffusion velocity method (Ogami and Akamatsu, 1991). Recently, attempts to apply the discrete vortex method to heat transfer (Ogami, 1997) and 3-dimensional flow analysis (Ro and Tsutahara. 1997) were reported.

The sea anchors are generally divided into 3 types according to their spread properties: horn type, corn type, and circular arc type. The circular arc type was used in this study since it has the largest drag coefficient, and 2-dimensional calculations of properties are available.

2. Calculation Method

2.1 Analytical Model and Boundary Condition

Fig. 1 shows an analytical model of a circular arc-type sea anchor. In Fig. 1, the center of the curvature of the sea anchor is the assumed origin of the coordinate system, and x- and y-axes are supposed to be in the reverse and vertical direction to the uniform flow U, respectively. θ represents the angle between the x-axis and each edge of the sea anchor, and R is the radius of curvature. Assuming the sea anchor to be a circular arc-type wing, which is zero in thickness, m numbers of bound vortices (○) are spaced at equal intervals, and the free vortices (●) are placed at half intervals of the bound vortices in the direction from each edge to the circumference. The complex potential $F(z)$, which represents the whole flow field around the sea anchor, is given by

$$F(z)=i\sum_{j=1}^{m}x_j\log(z-z_j)+i\sum_{\ell=1}^{n}\tilde{x}_\ell\log(z-\tilde{z}_\ell)-Uz \quad (1)$$

where i is the imaginary number ($\sqrt{-1}$) and x_j and z_j are the strength and position of m numbers of bound vortices, which represent the flow at the surface of the sea anchor, respectively. $\tilde{x}_\ell$ and

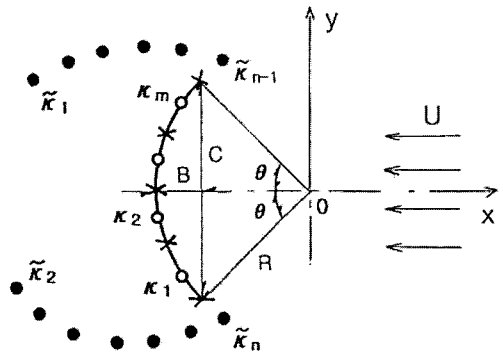

Fig. 1 An analytical model.

$\tilde{z}_\ell$ are the strength and position of n numbers of free vortices, which represent the separating shear layer, respectively. z is a position coordinate, which is a complex number ($=x+iy$)in this study. Since the vortices discharged from each edge of the sea anchor move in the wake, keeping their strength, the unknowns to be determined at each time step include the strength of m numbers of bound vortices, that of 2 numbers of free vortices, and stream function at the surface of the object. Therefore, the total number of unknowns to be determined is m+3. To solve the simultaneous equations, m+3 numbers of boundary conditions are required. At the centers between adjacent bound vortices, the conditions of the stream function Ψ at the control points of m+1,

$$\Psi = \Psi_0 = constant \tag{2}$$

Kelvin's circulation theorem,

$$\sum_{j=1}^{m} x_j + \sum_{\ell=1}^{n} \tilde{x}_\ell = 0 \tag{3}$$

and Kutta's condition at the lower or upper edge,

$$Real\{e^{i\theta} \cdot \frac{dF}{dz} \mid_{z=z_1}\} = 0 \tag{4}$$

$$Real\{e^{-i\theta} \cdot \frac{dF}{dz} \mid_{z=z_{m+1}}\} = 0 \tag{5}$$

are used where Real is the real part, dF/dz is complex velocity. In addition, z_1 and z_{m+1} are the locations at the lower and upper edges, respectively. Although the Kutta's condition can be applied to just one of the lower or upper edge, the conditions (4) and (5) are alternatively applied at each time step in consideration of theoretically perfect symmetry of the flow. When mapping the flow around the object to that around the circumference, the free vortices are also placed at the mirror positions, which are circulated in the reverse direction, in the circumference, satisfying the Kelvin's theorem. Therefore, Eq. (3) is not required here.

In a numerical calculation, a condition of velocity that a normal element of velocity of fluids at the surface of an object is identical with that of the object at that point, which is zero for a stationary object, is generally used as a boundary condition around the object. In addition, when analyzing the bound vortices that flow around a closed curved object, the number of control points is equal to that of bound vortices, which are unknowns. Since applying the Kelvin's theorem causes an imbalance where the number of conditions is higher than that of unknowns by 1, a control point must be omitted. However, when applying a condition of a stream function, the stream function Ψ_0 at the surface of an object becomes a unknown, preventing the imbalance described above.

When applying a free vortex to a separation point, the strength of the vortex is widely determined by using the Kutta's condition on the assumption that the vortex is introduced around the separation point or by using a boundary layer theory, in which the strength of the vortex $\tilde{x}_\ell = 1/(4\pi)v_s^2 \Delta t$, where v_s and Δt are the flow velocity at the separation

point and time step, respectively. The former method was used in this study. As shown in Fig. 1, an additional bound vortex was placed in direction to each edge of the sea anchor to discharge the bound vortex as a free vortex at each time step.

2.2 Simulation of Flow Field

The movement of a ℓ-th free vortex $\tilde{z}_\ell$ coming from each edge of the sea anchor is described by the following Euler's equation

$$\left.\begin{aligned} \tilde{z}_\ell\ (t+\Delta t\ ) &= \tilde{z}_\ell\,(t)+\overline{W}\cdot\Delta t \\ W&=\frac{d}{dz}\ [F(z)-i\,\tilde{\chi}_\ell \log(z-\ \tilde{z}_\ell)] \end{aligned}\right] \qquad (6)$$

where $^-$ is the complex conjugate, W is complex velocity obtained from the total of bound and free vortices in the flow field except for the ℓ-th free vortex, and Δt is a time step. At a non-viscous vortex, the induced velocity of the free vortex is in reverse proportion to the distance from the center. As shown in Eq. (6), as one free vortex approaches another or the surface of an object, unrealistic velocity is obtained. To avoid this inconsistency, therefore, the following viscous vortex model was used to determine the induced velocity v_θ.

$$v_\theta = \begin{cases} \dfrac{\chi}{r} & (r\geq\sigma) \\ \dfrac{\chi r}{\sigma^2} & (r<\sigma) \end{cases} \qquad (7)$$

where χ is strength of a vortex, r is a radius of the vortex, and σ is a radius of the core of the viscous vortex. Inamuro *et al.* (Inamuro, Saito and Adachi, 1984) used a so-called vortex core diffusion method, which expands σ in Eq. (7) in terms of time, to represent the viscous effect of fluids. However, since the diameter of sea anchors actually used on the sea is approximately 20m, and the flow field is in the area of a high Reynolds number, the effects of viscosity are expected to be low. Therefore, this study used the method to keep the radius of the vortex core constant. In other words, σ=0.025C on the basis of the distance between a control point and adjacent bound vortex.

Each streak line was calculated by inputting tracers through tracer sources, which are specific points on the upper flow, at every time step Δt. Eq. (6) was used for the movement of the tracers on the condition that $W=dF/dz$. For time line, the tracer sources were arranged on a straight line that was vertical to the upper flow, and the number of points was 60 in this study. The tracers were input at regular intervals, that is, $5\Delta t$ in this study. Their movement was identical with those of streak lines. The velocity vector field was calculated by constructing isotropic lattices in the flow field (20x15 at 0.2C intervals) and calculating the complex velocity at each lattice point. The stream line was obtained from the velocity vector field.

2.3 Coefficients of Lift and Drag

Assuming that, in Fig. 1, the fluid forces acting on the sea anchor in the direction of x-axis and y-axis are X and Y, respectively, applying the Blasius equation, which is expanded to unsteady flows, gives

$$X-iY=\frac{i\rho}{2}\oint_B\left(\frac{dF}{dz}\right)^2dz+i\rho\oint_B\frac{\partial\bar{F}}{\partial t}d\bar{z}$$
$$=2\pi\rho\left\{Ui\sum_{j=1}^{m}\dot{x}_j-\sum_{j=1}^{m}\sum_{\ell=1}^{n}\dot{x}_j\tilde{\dot{x}}_\ell\times\frac{1}{\tilde{z}_\ell-z_j}+i\sum_{j=1}^{m}\dot{x}_j\bar{z}_j+i\sum_{\ell=n-1}^{n}\frac{\tilde{x}_\ell}{\Delta t}\bar{\tilde{z}}_\ell\right\}\quad(8)$$

where ρ is the density of the fluid, B is the integral path on the surface of the sea anchor, and $\bar{}$ is the complex conjugate. $\dot{x}_j$ is the time difference, which is given by

$$\dot{x}_j=\frac{x_j(t)-x_j(t-\Delta t)}{\Delta t}\quad(9)$$

The $\ell=n-1$ and n at the last term in Eq. (8) are the free vortices newly produced from each edge of the sea anchor at each time step.

Assuming a span to be a length unit, the lift coefficient C_L and drag coefficient C_D, which describe the fluid dynamic properties of the sea anchor, are defined as

$$C_L=\frac{Y}{\frac{1}{2}\rho U^2C}\quad(10)$$

$$C_D=\frac{-X}{\frac{1}{2}\rho U^2C}\quad(11)$$

where ρ and C are the density of the fluid and chord of the sea anchor, respectively.

3. Numerical Results and Discussion

The conditions of the calculation in this study were: the chord of the sea anchor C=1, uniform flow U=1, the number of bound vortices m=20, and time step Δt = 0.1. The camber ratio B/C and dimensionless time Ut/C were used as variables to analyze the flow field. A personal computer (Model SPC8200PG manufactured by Samsung Electronics) was used for the calculation. The calculation time with a variable to 400 steps was 10 minutes for the fluid force and vortex distribution, 38 for the streak line, 25 for the time line, and 10 for the velocity vector and stream line. Since 2 new free vortices are created at each time step, a total of 800 free vortices were created in the flow field when the time steps reach 400.

When analyzing the flow field of a bluff body with the discrete vortex method or when describing viscous diffusion of fluids with the random-walk method, introduction of sufficient vortex elements are necessary for proper analysis of the flow field. The reason for the former is that vortex elements are placed all around such a bluff body due to the non-uniformity of its separation points, and subsequently the separation points are automatically determined due to the interaction of the vortex elements. The reason for the latter is that the method, which is based on a statistical perspective, is to describe the viscous diffusion effects by applying normal random numbers to position coordinates of each vortex element, in correspondence to Brownian movement. As for a sea anchor, however, it is possible to infer its separation points from its geometric shape, and the flow field is in an area of

which the Reynolds number is high. Therefore, as shown in the former studies (Inamuro, Saito and Adachi, 1984: Ro, 1993: Ro, 2000: Tsutahara, Kimura and Ro, 1989: and Tsutahara, Kimura and Ro, 1994), the number of vortex elements, used in this study, is sufficient to obtain qualitatively correct results.

Fig. 2 expresses the vortex distributions and stream lines at the case of the camber ratio B/C of 0.1, 0.3, and 0.5. Regardless of the camber ratio, counterclockwise vortices (●) were created at the upper edge, while clockwise vortices (○) were made at the lower edge. They formed large-sized Karman vortices at the wake side by turns. In addition, the interval of the Karman vortices slightly increased as the camber ratio was higher.

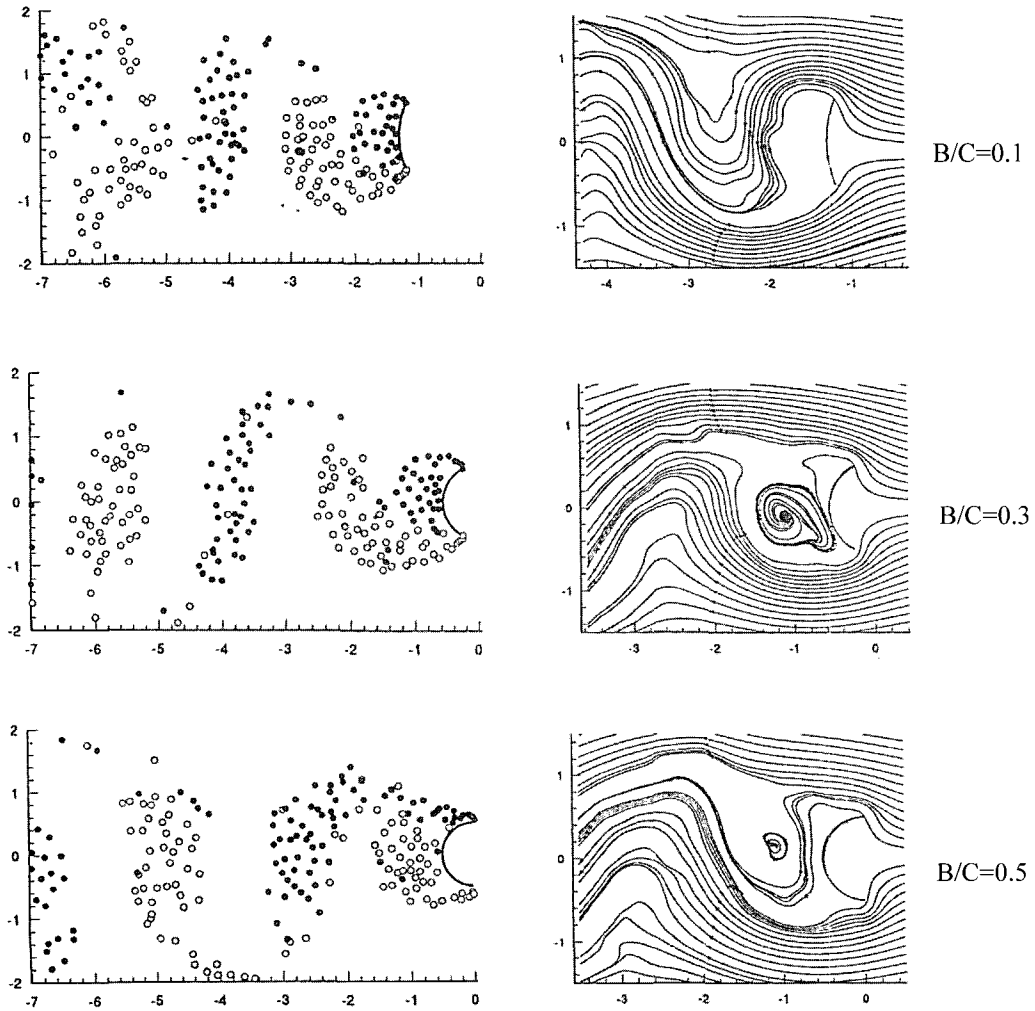

(a) Vortex distributions (b) Stream lines

Fig. 2 Flow patterns of various camber ratios (Ut/C=40).

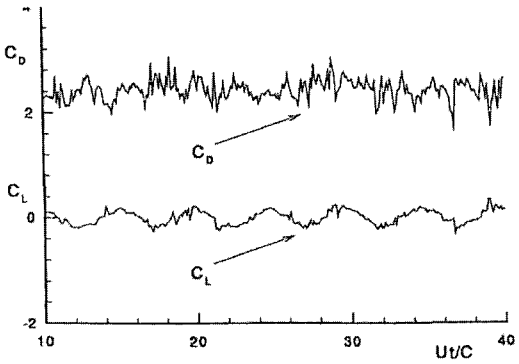

Fig. 3 Drag and lift coefficients with time (B/C=0.1).

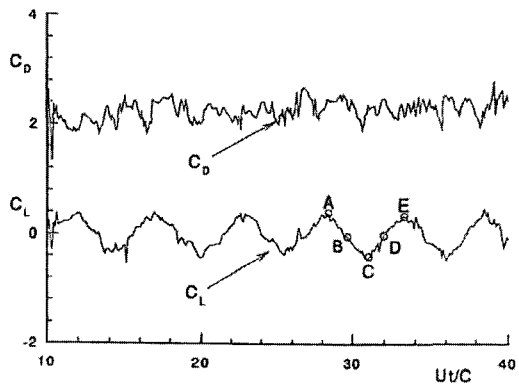

Fig. 4 Drag and lift coefficients with time (B/C=0.2).

Table 1 Drag coefficients(CD), lift coefficients (CL) and Strouhal numbers(St) for various camber ratios(B/C)

B/C	0.1	0.2	0.3	0.4	0.5
C_D	2.5	2.3	2.4	2.3	2.3
C_L	±0.25	±0.44	±0.60	±0.72	±0.88
St	0.208	0.196	0.204	0.187	0.185

Fig. 3 shows the variation of drag coefficient C_D and lift coefficient C_L with time when B/C=0.1. The drag coefficient showed little variation with time, while the lift coefficient fluctuated around 0.

Fig. 4 presents the variation of C_D and C_L with time when B/C=0.2. The variation is nearly identical with that in Fig. 3, qualitatively. However, when B/C was raised from 0.1 to 0.2, the drag coefficient slightly decreased, and the amplitude of the lift coefficient largely increased.

Table 1 describes the variation of drag coefficients C_D, lift coefficients C_L, and Strouhal numbers St with camber rations B/C. The results in the Table 1 were obtained by averaging each value, based on the range in which the flow was sufficiently developed,that is, the last 2 cycles of the lift coefficient, after calculating up to 400 time steps. The life coefficient was obtained by averaging the maximum and minimum values. The Strouhal numbers were calculated by the following equation: St=fC/U, where f is dimensionless frequency.

As shown in Table 1, as the camber ratio increased, the drag coefficient slightly decreased, the amplitude of the life coefficient significantly increased, and the Strouhal number slightly decreased. In other words, there was little variation of the drag coefficient and Strouhal number with the camber ratio, while the amplitude of the life coefficient largely depended on the camber ratio. These results indicate that, when designing a sea anchor, decrease in the camber ratio will significantly improve its dynamic stability without affecting other properties.

Fig. 5 shows the variation of vortex distributions and velocity vectors with time. A to E in Fig. 5 correspond to the points A to E on the lift coefficient curve in Fig. 4, respectively. Focusing on the

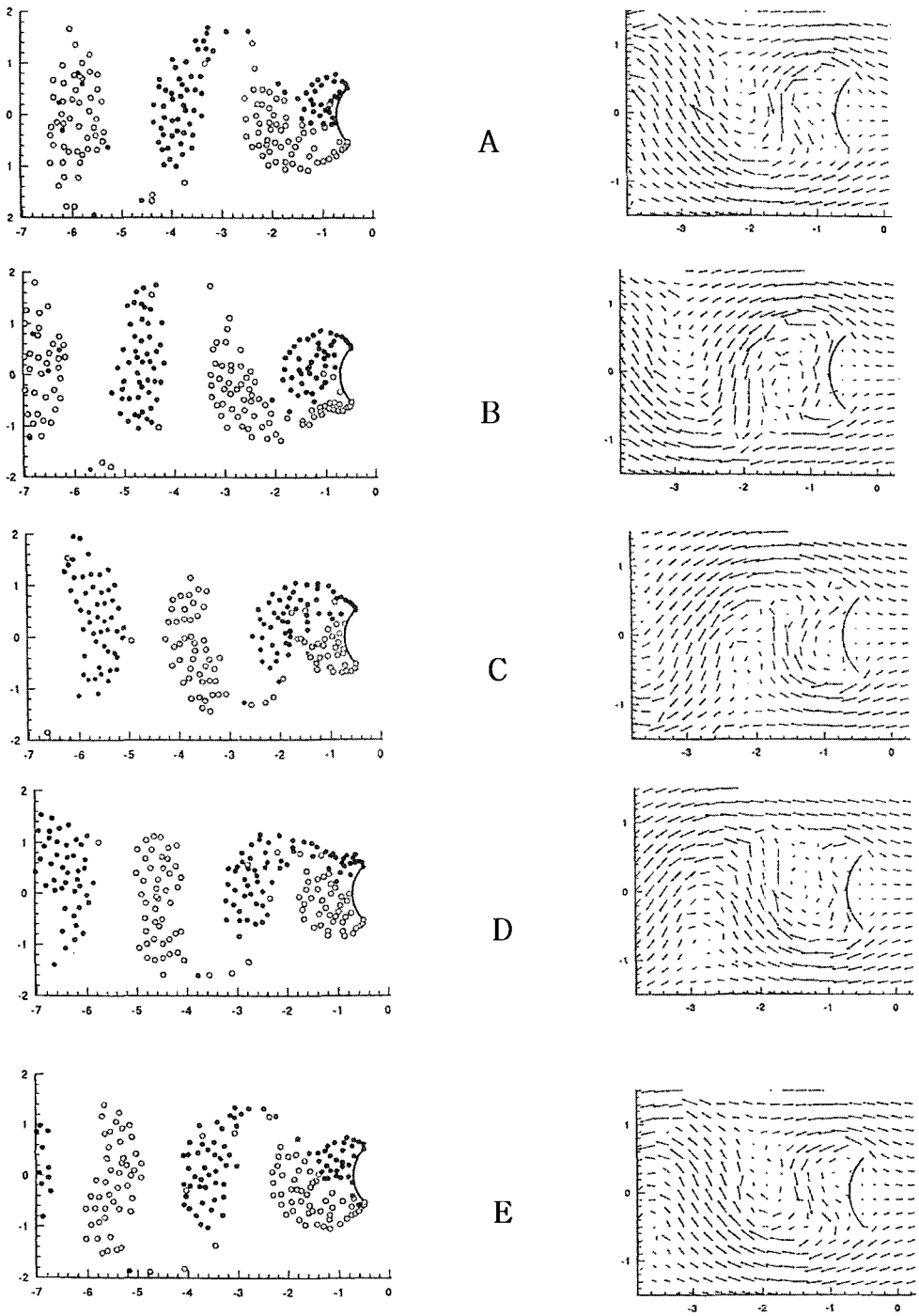

(a) Vortex distributions (b) Velocity vectors

Fig. 5 Flow patterns with time (A~E in the figure correspond to those points on Fig.4).

back face of the sea anchor, that is, the coordinates (-1,0), the back faces in A and B were occupied with the counterclockwise vortices (●)created at the upper edge, while those in C and D were filled with the clockwise vortices (○) formed at the lower edge. In addition, the vortex distributions at the point (A or E) of highest lift coefficient were contrary to those at the point (C) of lowest lift coefficient. In other words, from A to E, aggregates of vortices with + or - direction are created at the back face of the sea anchor by turns, and these form Karman vortices at regular intervals and flow toward the wake side. These Karman vortices result in the cyclic fluctuation of the life coefficient as shown in Fig. 4, causing the dynamic instability of the sea anchor. As shown in Fig. 5 (b), counterclockwise vortices were mostly created at A and B at the back face of the sea anchor, while clockwise vortices were mainly formed at C and D. The vortices around the coordinates (-1,0) at A gradually moved to (-1.2,0) at B, (-2,0) at C, (-2.8,0) at D, and (-3.6,0) at E.

Fig. 6 shows the variation of stream lines, streak lines, and time lines with time. A and C in Fig. 6 correspond to the maximum point A and minimum point C on the lift coefficient curve in Fig. 4, respectively. At both of the maximum and minimum points, the stream lines, streak lines, and time lines were symmetric with respect to the x-axis. In Fig. 6 (a), the interval of the stream lines was narrow around the upper edge at A and lower edge at C. Since, in general, flow velocity is high and pressure is low at the part of narrow intervals, lift is thought to act in the positive direction at A, while negative at C. In Fig. 6 (b) and especially (c), the center parts are in a bulging shape, indicating that the flow at the parts is slower than both sides. As shown in Fig. 6 (a) and (b) and Fig. 5 (b), the

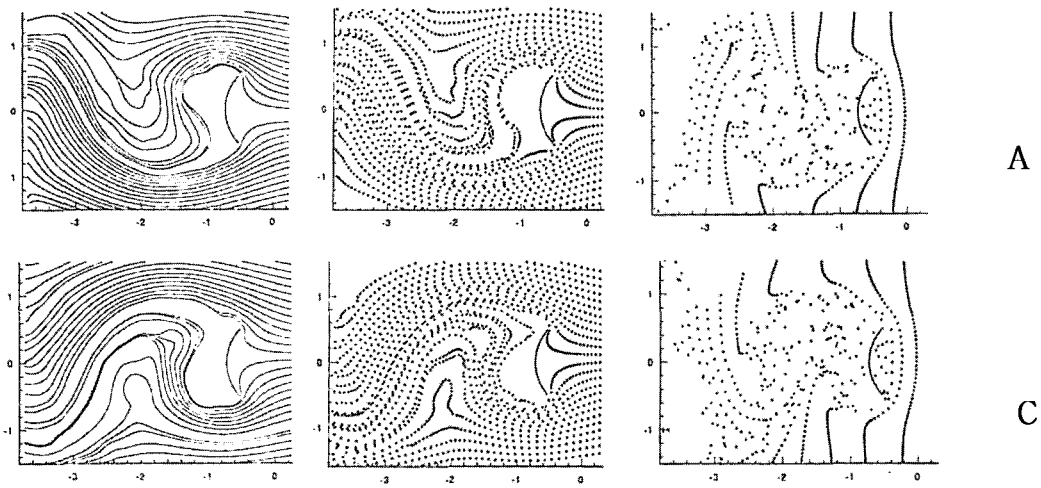

(a) Stream lines (b) Streak lines (c) Time lines

Fig. 6 Flow patterns with time (A and C on the figure correspond to those points on Fig.4).

stationary fluids at the driving face of the sea anchor gradually moved to both edges of that.

4. Conclusions

The dynamic characteristics of the unsteady flow of the circular arc-type sea anchor were clearly analyzed using the discrete vortex method. The flow around the sea anchor was described by placing the bound vortices at equal intervals, and the separation was assumed to occur at the upper and lower edges. The dynamic characteristics and flow fields of the sea anchor were determined with the variables of camber ratio and dimensionless time.

With the variation of time, the drag coefficient rarely changed, while the lift coefficient cyclically fluctuated. The reason for the cyclic fluctuation was the effects of the Karman vortices created at each edge. As the camber ratio increased, the drag coefficient and Strouhal number remained nearly constant, while the amplitude of the life coefficient significantly increased. The fluids at the driving face of the sea anchor stayed almost stationary.

The calculation using the discrete vortex method largely depended on the time step and the number of bound vortices. Therefore, it is required to further study to determine the optimal values of these variables.

Acknowledgements

This work was supported by the NURI and Brain Korea 21 Projects.

References

[1] Cho, T. H., Drawing of modern Korean fishing gear, *National Fisheries Research and Development Institute*, Gyeongnam, pp. 89-91, 1989.

[2] Chorin, A. J., "Numerical Study of Slightly Viscous Flow," *J. of Fluid Mechanics*, Vol.57, pp. 785-796, 1982.

[3] Inamuro, T. Saito, T. and Adachi, T., "A Numerical Analysis of Unsteady Separated Flow by the Discrete Vortex Method Combined with the Singularity Method," *Computer & Structure*, Vol.19, No.1-2, pp. 75-84, 1984.

[4] Kuwahara, K, "Numerical Study of Flow past an Inclined Flat Plate by an Inviscid Model," *J. of the Physical Society of Japan*, Vol.35, No.5, pp. 1545-1551., 1973.

[5] Lee, B. G., Park, S. W., and Kim, J. G., *Introduction of fishery in Korean waters*, Taehwa printing co., Pusan, pp. 112-116, 1985.

[6] Nomura, M., Mori, K., Tawara, Y. and Osawa, Y., "Hydraulic Resistance of Current Parachute," Bull. Tokai Reg. Fish. Res. Lab., No. 52, pp. 49-74, 1967.

[7] Ogami, Y. and Akamatsu, T., "Viscous Flow Simulation Using the Discrete Vortex Method - The Diffusion Velocity Method," *Computers and Fluids*, Vol.19, Pt.3, pp. 433-441, 1991.

[8] Ogami, Y., "Simulation of Natural Convecti-on by the Vortex Method for Heat Transfer," Japan Soc. of CFD, 11th Symposium paper, pp. 373-374, 1997.

[9] Sarpkaya, T., "An Analytical Study of Separated Flow about Circular Cylinders," Trans. of the ASME, *J. of Basic Engineering*, Vol.90, pp. 511-518, 1986.

[10] Sung, H. T., Kim, Y. N. and Hyun, J. M., "Discrete Vortex Simulation of Pulsating Flow Behind a Normal Plate," Trans. of the ASME, *J. of Fluids Engineering*, Vol.116, pp. 862-869, 1994.

[11] Tsutahara, M.,Kimura, T. and Ro, K. D., "Unsteady Pressure and Force in the Discrete Vortex Methods," Trans. of the Japan Society for Aeronautical and Space Sciences, Vol. 32, No.97, pp. 129-142, 1989.

[12] Ro, K. D., "Development of the Weis-Fogh Type Ship Propulsion Mechanism (Visualization and Numerical Analysis of the Flow Field)," *Transactions of the KSME*, Vol. 17, No. 2, pp. 426~437 in Korean, 1993.

[13] Ro, K. D., "Calculation of Thrust and Drag Characteristics for Ship's Propulsion Mechanism of Weis-Fogh Type," *KSME International Journal*. Vol. 14, No. 11, pp. 1257~1266, 2000.

[14] Ro, K. D. and Tsutahara, M., "Numerical Analysis of Unsteady Flow in the Weis-Fogh Mechanism by the 3D Discrete Vortex Method with GRAPE3A," *Transactions of the ASME, Journal of Fluids Engineering*, Vol. 119, pp. 96~102, 1997.

[15] Tsutahara, M., Kimura, T. and Ro, K. D., "Unsteady Pressure and Force in the Discrete Vortex Methods," *Transactions of the Japan Soc. Aero. Space Sci.* Vol. 32, No. 97, pp. 129~142, 1989.

[16] Tsutahara, M., Kimura,T. and Ro, K. D., "Ship's Propulsion Mechanism of Two-Stage "Weis-Fogh" Type," Trans. of the ASME, *Journal of Fluids Engineering*, Vol.116, pp.278-286, 1994.

Author Profile

Ki-Deok Ro

Date of birth : June 16, 1953.
Pukyong National University, 1973 to 1977, Bachelor of Marine Engineering.
Kobe University, 1984 to 1986, Master of Mechanical Engineering.
Kobe University, 1986 to 1989, Doctor of Mechanical Engineering.
Mobil oil Company, 1977 to 1979, Marine Engineer.
National Tongyeong Fisheries College, 1979 to 1995, Professor.
Gyeongsang National University, 1995 to present, Professor.

Se-Kyung Oh

Date of birth : March 6, 1948.
Pukyong National University, 1969 to 1973, Bachelor of Marine Engineering.
Pukyong National University, 1986 to 1988, Master of Marine Engineering.
Pukyong National University, 1997 to 2000, Doctor of Marine Engineering.
National Tongyeong Fisheries College, 1976 to 1995, Professor.
Gyeongsang National University, 1995 to present, Professor.